AGU PUBLICATIONS

JGR

Journal of Geophysical Research: Oceans

RESEARCH ARTICLE

10.1002/2015JC011084

Key Points:
- Elevated dissolved methane concentrations measured above Arctic seafloor seeps
- Methane released from seeps mainly lost via oxidation rather than mixing
- Release of methane to atmosphere mainly occurs on the shallow shelf

Supporting Information:
- Supporting Information S1

Correspondence to:
C. A. Graves,
Carolyn.Graves@noc.soton.ac.uk

Citation:
Graves, C. A., L. Steinle, G. Rehder, H. Niemann, D. P. Connelly, D. Lowry, R. E. Fisher, A. W. Stott, H. Sahling, and R. H. James (2015), Fluxes and fate of dissolved methane released at the seafloor at the landward limit of the gas hydrate stability zone offshore western Svalbard, *J. Geophys. Res. Oceans*, *120*, doi:10.1002/2015JC011084.

Received 26 JUN 2015
Accepted 14 AUG 2015
Accepted article online 19 AUG 2015

Fluxes and fate of dissolved methane released at the seafloor at the landward limit of the gas hydrate stability zone offshore western Svalbard

Carolyn A. Graves[1], Lea Steinle[2,3], Gregor Rehder[4], Helge Niemann[2], Douglas P. Connelly[5], David Lowry[6], Rebecca E. Fisher[6], Andrew W. Stott[7], Heiko Sahling[8], and Rachael H. James[1]

[1]Ocean and Earth Science, National Oceanography Centre, University of Southampton, Southampton, UK, [2]Department of Environmental Sciences, University of Basel, Basel, Switzerland, [3]GEOMAR, Helmholtz Centre for Ocean Research Kiel, Kiel, Germany, [4]Leibniz Institute for Baltic Sea Research Warnemünde, Rostock, Germany, [5]Marine Geoscience, National Oceanography Centre, Southampton, UK, [6]Department of Earth Sciences, Royal Holloway, University of London, Egham, UK, [7]Natural Environment Research Council Life Sciences Mass Spectrometry Facility, Centre for Ecology and Hydrology, Lancaster, UK, [8]Department of Geosciences, MARUM, Bremen, Germany

Abstract Widespread seepage of methane from seafloor sediments offshore Svalbard close to the landward limit of the gas hydrate stability zone (GHSZ) may, in part, be driven by hydrate destabilization due to bottom water warming. To assess whether this methane reaches the atmosphere where it may contribute to further warming, we have undertaken comprehensive surveys of methane in seawater and air on the upper slope and shelf region. Near the GHSZ limit at ~400 m water depth, methane concentrations are highest close to the seabed, reaching 825 nM. A simple box model of dissolved methane removal from bottom waters by horizontal and vertical mixing and microbially mediated oxidation indicates that ~60% of methane released at the seafloor is oxidized at depth before it mixes with overlying surface waters. Deep waters are therefore not a significant source of methane to intermediate and surface waters; rather, relatively high methane concentrations in these waters (up to 50 nM) are attributed to isopycnal turbulent mixing with shelf waters. On the shelf, extensive seafloor seepage at <100 m water depth produces methane concentrations of up to 615 nM. The diffusive flux of methane from sea to air in the vicinity of the landward limit of the GHSZ is ~4–20 μmol m^{-2} d^{-1}, which is small relative to other Arctic sources. In support of this, analyses of mole fractions and the carbon isotope signature of atmospheric methane above the seeps do not indicate a significant local contribution from the seafloor source.

1. Introduction

Seepage of methane from seafloor sediments on continental margins is widespread, but remains poorly quantified [*Boetius and Wenzhöfer*, 2013; *Judd and Hovland*, 2007]. Microbially mediated oxidation of methane in bottom waters near seep sites means that seawater is typically undersaturated with respect to the atmosphere [*Reeburgh*, 2007]. The oceans are therefore considered to make a minor contribution to the global atmospheric methane budget [*Kirschke et al*., 2013], with inputs from surface seawater only occurring in localized regions of surface supersaturation, for example, where methane is transported directly to the sea surface in the gas phase. However, new sites of seafloor methane seepage continue to be discovered [e.g., *Römer et al*., 2014; *Skarke et al*., 2014], and recent studies suggest that sea to air methane fluxes at some locations may be far higher than previously thought [e.g., *Shakhova et al*., 2010a]. Seepage of methane from seafloor sediments in the Arctic Ocean has been linked to release from temperature-sensitive shallow marine sediment reservoirs, including permafrost and methane hydrate [*Berndt et al*., 2014; *Ferré et al*., 2012; *Sahling et al*., 2014; *Shakhova et al*., 2014; *Westbrook et al*., 2009]. As Earth's climate continues to warm [*Intergovernmental Panel on Climate Change*, 2013], there is a need to constrain the potential for feedback between seafloor and atmospheric methane systems.

Methane hydrate is an ice-like solid in which methane is trapped in a cage of water molecules. It forms under specific high-pressure and low-temperature conditions where water is supersaturated with

methane [e.g., *Sloan and Koh*, 2008]. Naturally occurring submarine methane hydrate is estimated to contain ~500–2500 Gt of carbon globally [*Milkov*, 2004], mostly in continental margin sediments [*Krey et al*., 2009]. The presence of hydrate reduces sediment permeability such that subsurface gas flow can be directed along the base of the hydrate layer, with seepage at the seafloor in waters shallower than the landward limit of the hydrate stability zone [*Naudts et al*., 2006; *Schmale et al*., 2011]. Destabilization of methane hydrate in seafloor sediments is proposed to have contributed to previous episodes of major climate change, including the Paleocene-Eocene thermal maximum [e.g., *Dickens*, 2011], and recently discovered methane emissions from the seafloor offshore western Svalbard may, at least in part, be related to hydrate dissociation linked to warming of bottom waters [*Berndt et al*., 2014; *Biastoch et al*., 2011; *Reagan and Moridis*, 2009; *Thatcher et al*., 2013; *Westbrook et al*., 2009].

Methane that enters ocean bottom waters in bubble form rapidly dissolves and is subsequently diluted by mixing with overlying water masses, and dispersed by ocean currents. In the presence of oxygen, dissolved methane can be oxidized to carbon dioxide by aerobic methanotrophic bacteria [e.g., *Hanson and Hanson*, 1996] (equation (1)).

$$CH_4 + 2O_2 \rightarrow CO_2 + 2H_2O \quad (1)$$

The rate of aerobic methane oxidation (MOx) in the water column varies widely in time and space [*Mau et al*., 2013; *Steinle et al*., 2015], and the rate of bubble dissolution is mainly dependent on initial bubble size, water temperature and salinity, pressure, the presence of bubble coatings (organic material, or hydrate skin), and bubble rise velocity [*Leifer and Patro*, 2002; *Rehder et al*., 2009]. In water depths greater than 200 m, bubbles less than 10 mm in diameter are expected to dissolve before they reach the surface mixed layer, preventing direct venting of methane from seafloor seeps into the atmosphere [e.g., *Gentz et al*., 2014; *McGinnis et al*., 2006].

With the exception of CO_2, the biogeochemical transformations and physical processes that affect climatically active gases are poorly represented in coupled ocean-climate models. As seafloor methane seepage may increase in response to climate warming, particularly in the Arctic, observations of methane fluxes and oxidation rates and investigation of the processes that regulate them are critical. The discovery of more than 250 plumes of methane gas seeping from the seafloor at the landward limit of the gas hydrate stability zone (GHSZ) on the upper continental margin offshore western Svalbard [*Westbrook et al*., 2009] provides an ideal setting to address these issues. To this end, we have determined the distribution of methane in the water column in the vicinity of the landward limit of the GHSZ for three separate sampling campaigns. We use a simplified box model to quantify the fate of methane released from the seabed, and provide the first estimates of the sea-air methane flux for this area. Modeling indicates that vertical mixing into the surface mixed layer is slow, so oxidation of methane in the water column is the principal control on methane release to the atmosphere at the landward limit of the GHSZ.

2. Oceanographic Setting

The location of the methane seeps offshore western Svalbard is shown in Figure 1. The seafloor at the landward limit of the GHSZ is generally overlain by the warm saline Atlantic Water of the westward branch of the West Spitsbergen Current (WSC), which provides the primary influx of water and heat into the Arctic Ocean [e.g., *Aagaard et al*., 1987; *Saloranta and Haugan*, 2004; *Steinle et al*., 2015]. Both the mean temperature and speed of the WSC increase toward the shelf break [*Saloranta and Haugan*, 2004]. Deeper WSC waters to the west of this region loose heat and recirculate in the Fram Strait, while shallower WSC waters to the east of the region are subject to horizontal mixing across a density-compensated halocline near the shelf edge [*Cottier and Venables*, 2007; *Saloranta and Svendsen*, 2001] as well as less important vertical mixing and heat loss to the atmosphere [*Fahrbach et al*., 2001]. North of Svalbard, the WSC splits into two branches, with shallower waters ($<\sim$1000 m) continuing along the shelf edge and deeper waters moving along the western edge of the Yermak Plateau [*Schauer et al*., 2004]. On the continental shelf east of the landward limit of the GHSZ, the slower East Spitsbergen Current (ESC) carries fresher and colder polar water northward. Surface waters in the vicinity of the methane seeps typically consist of relatively fresh Arctic Water, which penetrates to deeper depths toward the coast [*Saloranta and Svendsen*, 2001] and may mix with WSC water [*Steinle et al*., 2015].

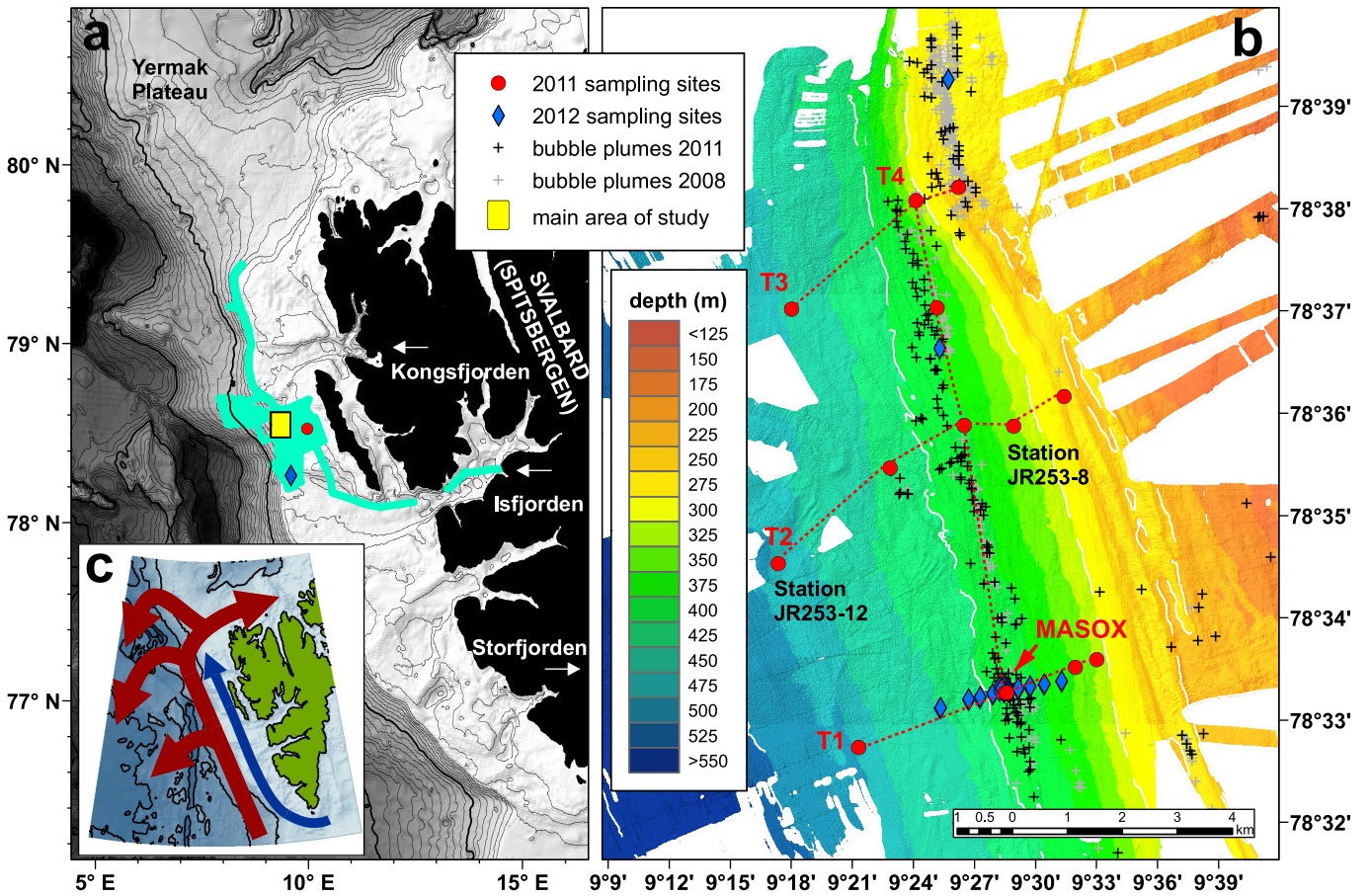

Figure 1. Map of the study area and water column sampling sites. Bathymetry in Figure 1a is from the GEBCO_08 Grid version 20100927 (http://gebco.net), contour interval is 100 m; light blue indicates He-386 cruise track, and yellow rectangle indicates the area expanded in Figure 1b, showing shipboard bathymetry from cruise JR253. Red circles show positions of cruise JR253 sampling stations; red lines indicate sampling transects T1–T4. Blue diamonds show sampling stations from cruise MSM21/4. Locations of seafloor bubble seeps identified by shipboard sonar during sampling are indicated by crosses. (c) The dominant direction of the main ocean currents in this region: the West Spitsbergen Current (WSC) in red, and the East Spitsbergen Current (ESC) in blue, modified from *Saloranta and Svendsen* [2001].

3. Sampling and Analytical Methods

3.1. Sample Collection

Seawater and air samples were collected from the vicinity of the methane seeps on RRS *James Clark Ross* cruise JR253 (7–23 July 2011), and on RV *Maria S. Merian* cruise MSM21/4 (18 July 2012 to 4 August 2012). Water column sampling was conducted in "clean ship" mode (i.e., no discharge of waste water, no smoking on deck) to minimize the potential for sample contamination. Seawater sampling sites are shown in Figure 1 and listed in supporting information Tables S1 and S2, and air sampling sites are shown in supporting information Figure S1. Bubble plumes were identified by shipboard sonar: a Simrad EK60 "fish-finder" sonar (38, 120, and 200 kHz) and a 12 kHz Simrad EM122 sonar were used on the RRS *James Clark Ross* [*Westbrook et al*., 2009], and a PARASOUND sonar (18 kHz parametric echo sounder) was used on the RV *Maria S. Marian* [*Berndt et al*., 2014]. In 2012, an equilibrator system [*Gülzow et al*., 2011] was used to continuously measure surface water methane concentrations along the cruise track of RV *Heincke* during cruise He-387 (20 August 2012 to 6 September 2012; the area covered by the cruise track is shown in Figure 1a [*Sahling et al*., 2014]).

In 2011, seawater samples were taken along three transects (T1–T3; Figure 1b) of ~6 km in length, extending from ~200 m water depth through the area of methane seepage at ~400 m water depth, to water depths of ~500 m. Each transect consisted of three to five vertical profiles. In 2012, the central segment of transect T1 was sampled more intensively [*Steinle et al*., 2015]: twice as a 10 vertical profile transect, once with 5 vertical profiles near the central point, and twice by a single vertical profile at the central point,

culminating in 27 vertical profiles representing five sampling time points over 16 days. An additional station located ~30 km south of the main study area at ~300 m water depth was also sampled (Figure 1a).

Seawater was collected in 10 L Niskin bottles mounted on a 24-bottle rosette frame fitted with a Seabird SBE911 conductivity-temperature-depth (CTD) sensor (Seabird Scientific). Samples for methane analysis were collected immediately upon recovery of the rosette frame into 1 and 0.5 L triple-layer Evarex Barrier Bags (Oxford Nutrition, UK), which had been flushed twice with nitrogen [*Berndt et al*., 2014; *Steinle et al*., 2015]. Samples for methane isotopes were taken into 125 mL glass vials with crimp seal tops, and poisoned with 2 mL saturated mercuric chloride solution (MSM21/4, MASOX site only). Quadruplicate samples for methane oxidation rate measurements were collected in 20 mL crimp-top vials, and filled bubble free (MSM21/4 only). Water was introduced to the equilibrator system on RV *Heincke* using the ship's underway pumped water system; the pump inlet was located 2.8 m below the sea surface. Air samples were collected as described in *Fisher et al*. [2011], from the ship's bridge (~16 and 29 m above sea level for JR253 and MSM21/4, respectively) by directing a hose into the direction of incoming wind and pumping into 5 L Tedlar bags.

3.2. Analytical Methods

Methane concentrations were determined using a headspace technique as described previously [*Berndt et al*., 2014; *Steinle et al*., 2015]. Briefly, 20 mL of N_2 was added to each sample bag and mixed vigorously. Seawater was equilibrated with the headspace gas for several hours before 2 mL of gas was subsampled for analysis by gas chromatography (Agilent 7890A, 6 ft, 2 mm i.d.; 80/100 mesh HayeSep Q packed stainless steel column, flame ionization detector). Seawater methane concentrations were calculated from headspace concentrations according to *Wiesenburg and Guinasso* [1979]. Analytical reproducibility was $<\pm 5\%$, determined by analysis of triplicate subsamples from the same Niskin bottle. The carbon isotopic composition of dissolved methane in seawater was determined at the Natural Environment Research Council Life Science Mass Spectrometry Facility's Lancaster Node (Lancaster, UK) by addition of ~20 mL helium headspace to samples with simultaneous removal of seawater, and subsequent analysis by isotope ratio mass spectrometry (Isoprime Ltd. Trace Gas Preconcentrator). Reproducibility of replicate standards was $< \pm 0.3‰$.

MOx rates were measured by radio-tracer assay as described previously [*Berndt et al*., 2014; *Niemann et al*., 2015; *Steinle et al*., 2015]. Briefly, water samples were incubated ex situ with trace amounts of ^{3}H-labeled CH_4 and the activities of ^3H_2O produced (cf equation (1)) as well as the residual ^{3}H-labeled CH_4 were measured by wet scintillation counting. MOx rate constants (k_{MOx}) were calculated from the fractional turnover of the tracer, assuming first-order rate kinetics.

The equilibrator system measured methane concentrations in air equilibrated with surface seawater by off-axis integrated cavity output spectroscopy (oa-ICOS, Los Gatos Research MCA), using a system almost identical to that described in *Gülzow et al*. [2011]. The ship's clean seawater system was maintained at a flow rate of >20 L min^{-1}, from which the supply for the equilibration system was branched off, assuring a high flow rate and low water residence time to minimize the potential for contamination. Data are only reported for when the ship was in transit (i.e., at speeds >4 knots) to exclude any analyses that could have been affected by ship contamination or ship-induced vertical entrainment of water from below the thermocline. The response time of the system for methane is ~10 min, and the precision of the measurements, assessed with gas calibration standards, was better than $\pm 0.1\%$ [*Gülzow et al*., 2011]. A detailed description of the equilibrator system and analytical setup is given in *Gülzow et al*. [2011].

Methane mole fractions and δ^{13}C-CH_4 in air were determined at Royal Holloway University of London by cavity ring-down spectroscopy (Picarro G1301) and trace gas-continuous flow gas chromatography isotope ratio mass spectrometry (Isoprime Ltd.) [*Fisher et al*., 2006], respectively. The precision of δ^{13}C-CH_4 measurements based on multiple ($n > 3$) analyses of secondary standards and samples for both cruises was better than $\pm 0.05‰$.

3.3. Box Model

A simplified box model was used to assess the relative importance of chemical and physical processes which modify the dissolved methane concentration in a parcel of water above the seep site, as that parcel of water is transported away from the seeps by the strong local bottom water currents. The processes considered in the model are: (i) aerobic oxidation (MOx), (ii) isopycnal mixing, and (iii) diapycnal mixing. Input

of methane from the seeps and advective transport are not explicitly considered, because the parcel of water moves away from its origin during the modeled time interval. The box is defined to represent the portion of the water column into which methane bubbles dissolve: the height of the box is given by the depth at which essentially all methane has dissolved (75 m), based on measurements of dissolved methane concentration (section 4.1), and bubble modeling [*Gentz et al*., 2014], while the footprint of the box is defined by the cross-slope (approximately east-west) width of seafloor affected by methane seeps (450 m) per meter along the ~400 m bathymetric contour. The dissolved methane concentration in the box therefore represents the average input of methane from all seeps in a 1 m segment along the ~400 m bathymetric contour.

The change in dissolved methane concentration with time after bubble dissolution is given by:

$$\delta C/\delta t = -\left[\delta C_{MOx} + \delta C_{I(west)} + \delta C_{I(east)} + \delta C_D\right]/\delta t \quad (2)$$

where C is methane concentration in mol m^{-3}, and *I(west)* is offshore isopycnal mixing, *I(east)* is onshore isopycnal mixing, and D is upward diapycnal mixing. The rate of methane oxidation is assumed to be first order, with a concentration ($C(t)$)-independent rate constant k_{MOx} in s^{-1}:

$$\delta C_{MOx}/\delta t = -k_{MOx} \cdot C(t) \quad (3)$$

Isopycnal and diapycnal mixing (turbulent diffusion) are described by Fick's first law of diffusion following e.g., *Mau et al*. [2012]:

$$\delta C_I/\delta t = -x^{-1} \cdot D_I \cdot (\Delta C(t)/\Delta x) \text{ and } \delta C_D/\delta t = -z^{-1} \cdot D_D \cdot (\Delta C(t)/\Delta z) \quad (4)$$

where x is the width of the box (450 m), z is the height of the box (75 m), and $\Delta C(t)/\Delta x$ and $\Delta C(t)/\Delta z$ are the methane concentration gradients away from the seep site in mol m^{-4} in the horizontal (x) and upward vertical (z) directions, and D_I and D_D are the isopycnal and diapycnal turbulent diffusion coefficients in $m^2\ s^{-1}$. Isopycnal mixing is assessed by analysis of methane concentration gradients toward the west (offshore) and east (onshore) (see Table 1). Isopycnal mixing in the north-south direction is neglected because the methane seeps are aligned with the bathymetric contours (approximately north-south), and because the dominant current is barotropic and northward so the diffusion term is small relative to advection of bottom waters. In support of this, the methane concentration gradient in the north-south direction is small. Because the bottom of the box is defined to be the seafloor, there is no downward diapycnal mixing.

The initial concentration of methane in the box was estimated by depth-averaging measured concentrations in the lower 75 m of the water column. The measured oxidation rate constants were similarly averaged, as were concentrations outside the box (away from the study area and in the upper water column). No correlation between methane concentration and k_{MOx} was observed in the study area as microbial activity was mainly dependent on the community size of methane oxidizers [*Steinle et al*., 2015]. However, no downstream measurements were made, so any evolution of oxidation rate constants as bottom water is advected northward is unconstrained.

A range of isopycnal and diapycnal mixing coefficients have been reported in the literature. We choose an isopycnal coefficient of $0.07 \pm 0.04\ m^2\ s^{-1}$ as calculated for length scales of 0.1–1 km based on a tracer study with sulfur hexafluoride at ~310 m water depth in the Atlantic Ocean [*Ledwell et al*., 1993, 1998]. This is much lower than the value of ~1000 $m^2\ s^{-1}$ calculated for longer length scales [*Ledwell et al*., 1998; *Sundermeyer and Price*, 1998]. When combined with the observed methane concentration gradients, the larger coefficient (1000 $m^2\ s^{-1}$) leads to isopycnal mixing rates larger than the rate of methane input from the seafloor seeps [*Sahling et al*., 2014] meaning that methane would not accumulate in seawater above the seeps, which is clearly inconsistent with our observations. The choice of a low isopycnal mixing coefficient is further supported by *Largier* [2003], who show that mixing decreases in nearshore environments from 1000 $m^2\ s^{-1}$ at 100–1000 km away from the coast to 0.1–100 $m^2\ s^{-1}$ at 0.1–10 km from the coast. Coefficients of diapycnal mixing are typically $10^{-7}-10^{-8}$ times lower than coefficients for isopycnal mixing [*Deng et al*., 2014]. Based on the water depth and latitude of our site [*Deng et al*., 2014], we used an upper limit for the diapycnal mixing coefficient of $10^{-3}\ m^2\ s^{-1}$ as measured in tracer experiments in bottom waters in the abyssal ocean [*Ledwell et al*., 2000]. Where measured, Arctic Ocean vertical mixing is typically very small, except in the immediate vicinity of topographic features [*Rippeth et al*., 2015; *Shaw and Stanton*, 2014] such

Table 1. Box Model Input Parameters[a]

Parameter	Symbol	Units	Value	Description
Box height	z	m	75	Height of box above seafloor: assumed depth interval within which all seafloor dissolves
Box width	x	m	450	Width of box: approximate width of seafloor affected by methane seepage perpendicular to the 400 m bathymetric contour
Initial methane concentration in box	$[CH_4]_i$	nM	93	Initial methane concentration: average methane concentration within 75 m of the seafloor measured in 2012
Oxidation rate constant	k_{MOx}	day^{-1}	0.016	Oxidation rate constant: average value measured in bottom waters in 2012
Standard deviation			0.01	
Minimum			0.0009	Depth-integrated single profile average for bottom 75 m of the water column
Maximum			0.04	Depth-integrated single profile average for bottom 75 m of the water column
Initial offshore concentration gradient	$(\Delta C/\Delta x)_W$	nM m^{-1}	0.05	Offshore concentration gradient: measured between seep sites aligned along the 400 m bathymetric contour and station JR253-12
Initial onshore concentration gradient	$(\Delta C/\Delta x)_E$	nM m^{-1}	0.09	Onshore concentration gradient: measured between seep sites aligned along the 400 m bathymetric contour and station JR253-8
Initial vertical concentration gradient	$(\Delta C \Delta x)_Z$	nM m^{-1}	0.06	Vertical concentration gradient: measured above and below 75 m above the seafloor at seep sites aligned along the 400 m bathymetric contour

[a]Methane oxidation rate constant data are shown in supporting information Figure S2.

as the Yermak Plateau where values up to 2.5×10^{-4} m^2 s^{-1} were determined [*Padman and Dillon*, 1991], validating our choice of upper limit mixing coefficient. The uncertainty in the values of these coefficients is taken into account in the model output, but we stress that, as these uncertainties are large, our model must be considered to be qualitative/semiquantitative, rather than fully quantitative.

3.4. Sea-Air Fluxes

The flux of methane from surface waters to the atmosphere is given by:

$$\text{Flux} = k\left([CH_4]_{surface} - [CH_4]_{equilibrium}\right) \quad (5)$$

where k is the gas transfer velocity and $[CH_4]_{surface}$ and $[CH_4]_{equilibrium}$ are, respectively, the measured concentration of methane in surface seawater and the calculated concentration of methane in surface seawater at equilibrium with the atmosphere [*Liss and Slater*, 1974; *Wanninkhof et al.*, 2009]. The equilibrium concentration is calculated from the total atmospheric pressure and the partial pressure of methane in dry air using the Bunsen solubility coefficient of methane at the temperature and salinity of surface seawater [*Wiesenburg and Guinasso*, 1979].

The gas transfer velocity (k) can be estimated from the molecular diffusivity (D) of the gas, the kinematic viscosity of seawater (μ), and the atmospheric wind speed at a height of 10 m (u_{10}) [*Wanninkhof*, 1992; *Wanninkhof et al.*, 2009]. D and μ are combined in the Schmidt number ($Sc = \mu/D$), such that:

$$k = 0.24 \cdot u_{10}^2 \cdot (Sc/660)^{-1/2} \quad (6)$$

where k has units of cm h^{-1} and u_{10} is in m s^{-1} [*Wanninkhof et al.*, 2009]. Further details of this calculation and choice of k parameterization are given in the supporting information Text S1 and Tables S3 and S4. Briefly, different k parameterizations [*Liss and Merlivat*, 1986; *McGillis et al.*, 2001; *Nightingale et al.*, 2000; *Wanninkhof*, 1992] yield overall sea-air fluxes ranging from 20% to 35% lower and 30% to 75% higher, depending on the wind speed.

Measured wind speeds were corrected for ship speed and direction of travel, as well as the height of measurement (z_{meas}) above the sea surface using the relationship $u_{10} = u_{measured} \cdot (z_{meas}/10)^{-0.11}$ [*Hsu et al.*, 1994]. Methane fluxes were only calculated using wind speed measurements from within 1 km of the seafloor seeps. The effects of temporal variability in wind speed on the sea-air flux were assessed by bin averaging wind speed in 1 m s^{-1} intervals.

Fluxes were calculated from measurements of the methane concentration in the water samples and estimates of the equilibrium methane concentration and gas transfer velocity. The equilibrium methane concentrations were calculated from surface seawater temperature and salinity, and the average measured atmospheric methane partial pressure and total atmospheric pressure during water sampling. Gas transfer

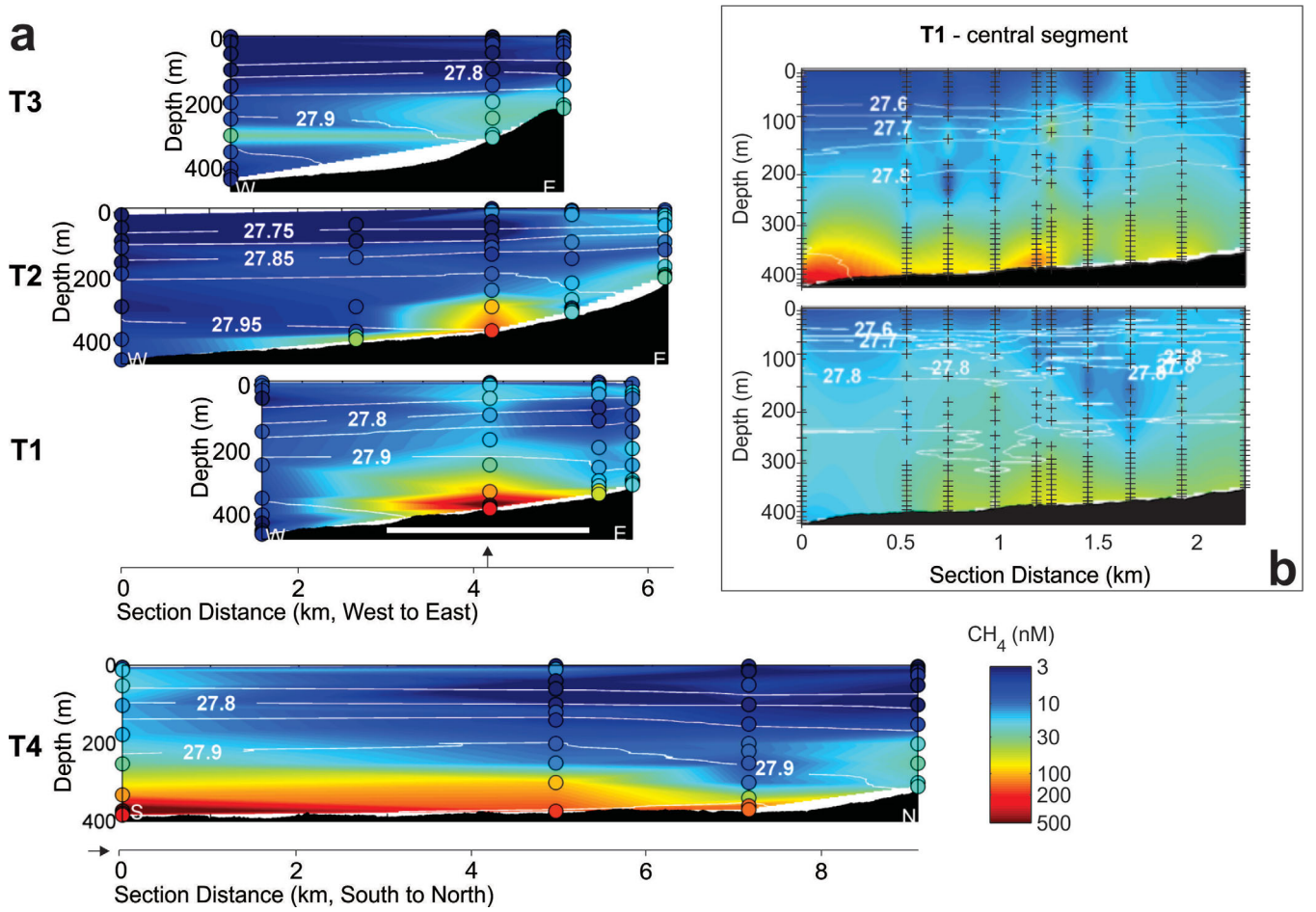

Figure 2. (a) Distribution of methane along east-west transects T1–T3, and north to south along transect T4 (see Figure 1 for transect locations). Sampling points are shown by the open circles. Contours show the density anomaly (σ_θ; kg/m^3). (b) The central segment of T1 (indicated by the white bar in Figure 2a) sampled on two further occasions at higher spatial resolution [from *Steinle et al.*, 2015]. Sampling points are shown by crosses.

velocities were calculated for the wind speed distribution observed during the measurement period, and measured surface seawater temperature. Detailed information on the uncertainty of these fluxes can be found in the supporting information Text S2 and Table S5. Briefly, variations in atmospheric methane mole fraction, atmospheric pressure, and surface seawater temperature and salinity lead to uncertainties in methane fluxes of $<\pm$10%. The most significant contribution to this uncertainty is the variation in the methane concentration of surface seawater, which is $\pm$30–40%.

Fluxes were also calculated for the equilibrator surface seawater methane concentration data. This data set provided simultaneous measurement of wind speed, surface seawater methane concentration, temperature and salinity, and atmospheric pressure. Fluxes were therefore calculated for each individual concentration measurement (5 s intervals). Atmospheric methane mole fractions were not simultaneously measured, so the average value of the air samples collected in 2012 was used. This contributes less than $\pm$5% to the overall uncertainty of the sea-air flux.

4. Results and Discussion

4.1. Distribution of Dissolved Methane

The distribution of methane in the water column in 2011 is shown Figure 2a. Highest methane concentrations are found close to the seafloor, in the methane seepage region at ~400 m water depth. This pattern is also observed in higher depth-resolution measurements made in 2012 (Figure 2b), and concentrations are

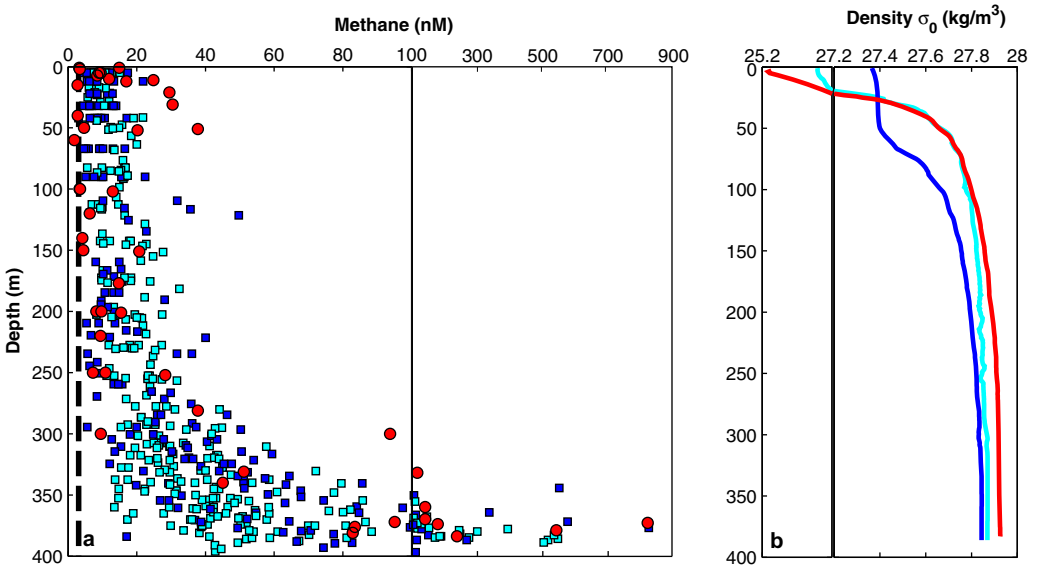

Figure 3. Profiles of (a) dissolved methane concentration and (b) density anomaly at the landward limit of the GHSZ. Circles (red) are data from 2011, and squares (blue) are data from 2012. The atmospheric equilibrium methane concentration (~3 nM) is shown by the vertical dashed black line. Density profiles shown are representative for methane concentrations of the corresponding colors.

consistent with previously published values for the shelf and shelf break offshore western Svalbard [*Berndt et al.*, 2014; *Damm et al.*, 2005; *Gentz et al.*, 2014; *Knies et al.*, 2004; *Steinle et al.*, 2015; *Westbrook et al.*, 2009].

The variation in the concentration of methane with depth in the vicinity of the methane seeps (i.e., close to the landward limit of the GHSZ) is consistent throughout the study area, and there are no obvious differences in either methane concentrations or the shape of the depth profiles measured in 2011 and 2012 (Figure 3). Average methane concentrations in the upper ~250 m of the water column are ~6 times lower than those in in bottom waters, and far less variable (2–50 nM compared to 6–820 nM). Nevertheless, the entire water column is supersaturated with respect to the atmospheric equilibrium (~3 nM CH_4, section 4.2.3).

At distances of <3 km from the seafloor methane seeps, there is no correlation between the methane concentration of near-surface waters ($\sigma_\theta < 27.5$ kg m^{-3}) and distance from the seeps. The average methane concentration of surface seawater collected by Niskin bottles was ~5 nM (range 3–9 nM) in 2011 and ~11 nM (range 4–17 nM) in 2012. The average concentration measured by the equilibrator system, which covered a much larger area with less specific focus on water overlying identified seep sites, was slightly lower at 4.7 nM (range 3.1–6.4 nM). In addition to representing different spatial coverage of the study site, the concentration difference between the two surface water data sets may reflect sampling depths: on average, "surface" seawater collected by Niskin bottles was slightly deeper (~1–12 m below the sea surface), than "surface" seawater sampled by the equilibrator system (~2.8 m below the sea surface). Similar differences between methane concentrations measured in Niskin bottle samples and in seawater measured using an equilibrator system have also been reported in the Gulf of Mexico [*Hu et al.*, 2012; *Solomon et al.*, 2009].

Our measurements show that surface waters are methane supersaturated with respect to the atmospheric equilibrium not only in the immediate vicinity of the seafloor methane seeps, but up to at least 35 km to the west of the landward termination of the GHSZ, 80 km to the north, and 15 km to the south (Figure 4). Highest surface water methane concentrations (52 nM) are observed at shallow water depths (<100 m) on the continental shelf, while surface waters are closest to atmospheric equilibrium at the site furthest offshore (~800 m water depth), suggesting that water depth is an important control on sea-air methane flux.

4.2. Fluxes, Sources, and Fate of Dissolved Methane in the Water Column Offshore Svalbard

4.2.1. Loss of Methane From Bottom Waters

High concentrations of dissolved methane are restricted to the lower 75 m of the water column (Figures 2 and 3). Bubble observations and modeling offshore western Svalbard and elsewhere indicate that

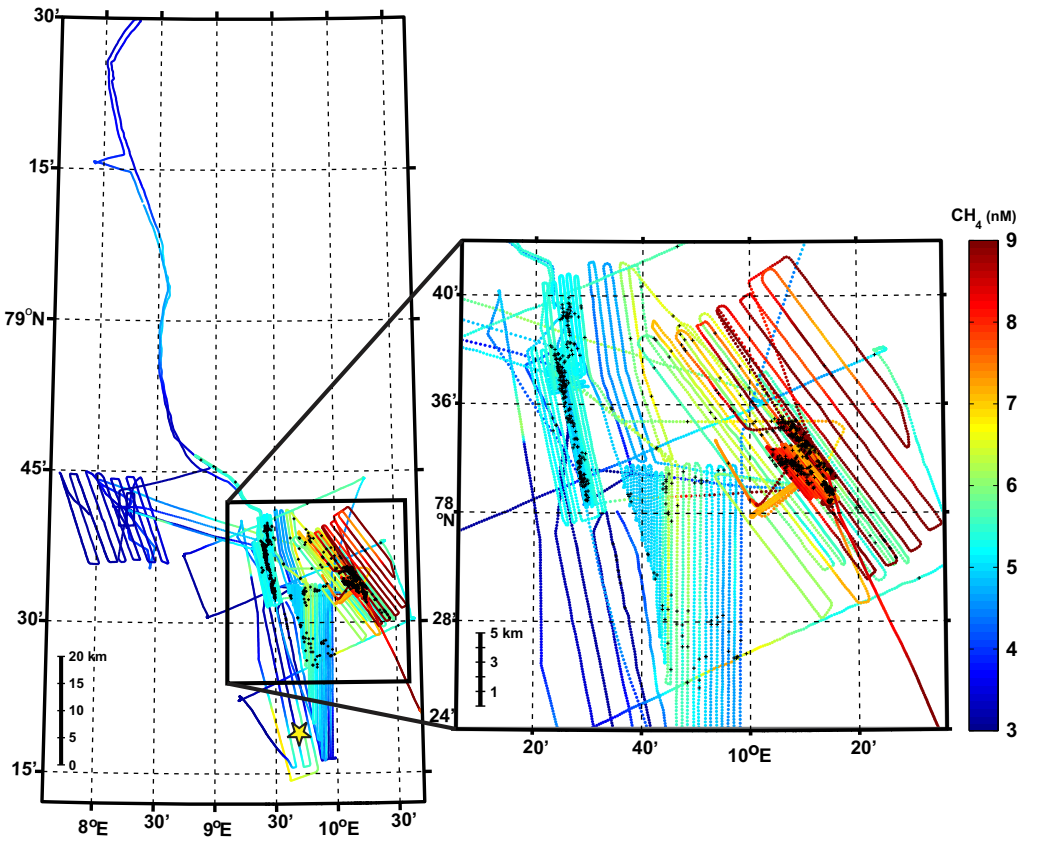

Figure 4. Methane concentration in surface seawater measured using the equilibrator system during RV *Heincke* cruise He-387. Black crosses show the location of seafloor methane seeps mapped during the cruise [*Sahling et al*., 2012, 2014]. Yellow star indicates the position of the depth profile sampling station (cruise MSM 21/4) to the south of the main study area.

essentially all methane released in bubbles can be expected to dissolve in this depth zone [*Gentz et al*., 2014; *Leifer and Patro*, 2002; *Schneider von Deimling et al*., 2011; *Westbrook et al*., 2009]. As soon as the methane is in the dissolved phase, it is subject to microbially mediated aerobic oxidation, advection by water currents, and turbulent diffusion across concentration gradients. The proportion of methane released at the seafloor which reaches the upper water column depends on the relative rates of these processes, and may be estimated using our simplified box model.

The results of the model are shown in Figure 5, and input parameters are given in Table 1, with additional details provided in supporting information Table S6. There are large uncertainties associated with all methane flux terms, as the isopycnal and diapycnal mixing coefficients are poorly constrained, and the measured methane oxidation rate constants are highly variable in both space and time because MOx-activity is controlled by the standing stock of aerobic methanotrophs, which is strongly influenced by variations in the WSC (supporting information Figure S2) [*Steinle et al*., 2015]. Based on average observed conditions and best estimates for mixing coefficients, a parcel of bottom-water retains elevated (above-background) dissolved methane concentrations for approximately 150 days after it is advected away from the site of seafloor methane input by bottom water currents.

Model results indicate that oxidation is a key control on methane concentrations, consuming ~60% of the methane released at the seafloor before it is mixed outside of the box (Figure 5f). An additional ~27% of methane is removed by isopycnal mixing. Upward diapycnal mixing between deep and surface waters accounts for removal of only 9% of methane released at the seafloor, which means that most of the methane released at the seafloor is unlikely to be released into the atmosphere. These results are in agreement with global ocean biogeochemical models, which simulate methane release into Arctic bottom waters as a result of methane hydrate dissociation [*Elliott et al*., 2011].

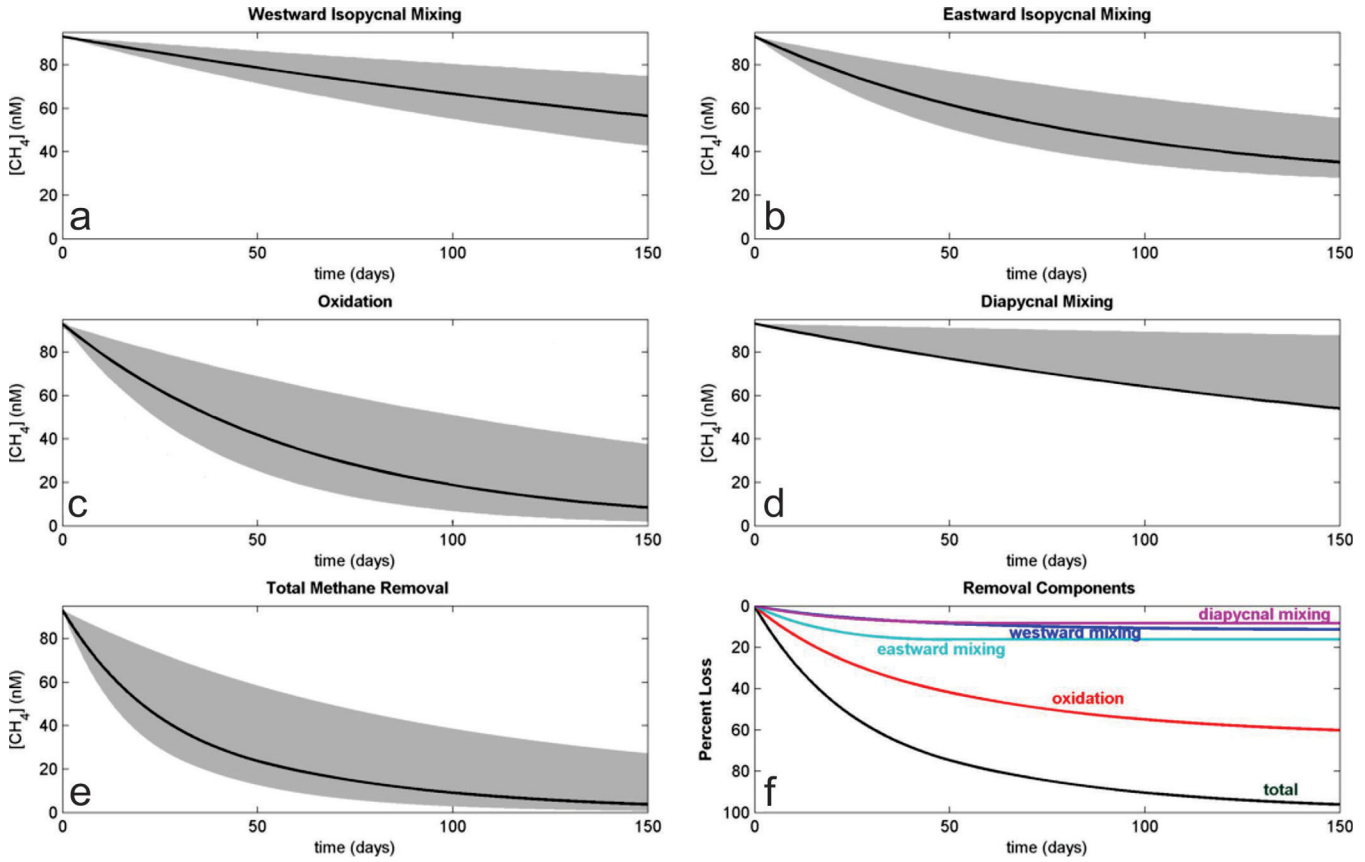

Figure 5. Loss of methane from bottom waters due to (a) offshore isopycnal mixing, (b) onshore isopycnal mixing, (c) oxidation, and (d) upward diapycnal mixing, calculated using the box model. The grey shaded regions represent the uncertainty in fluxes due to the uncertainty in the rate constants. These are: isopycnal mixing coefficient ± 0.04 m^2 s^{-1}, diapycnal mixing coefficient $10^{-4}-10^{-3}$ m^2 s^{-1}, and k_{MOx} ± 0.01 day^{-1}. (e) The total methane removal, and (f) the relative loss due to each term.

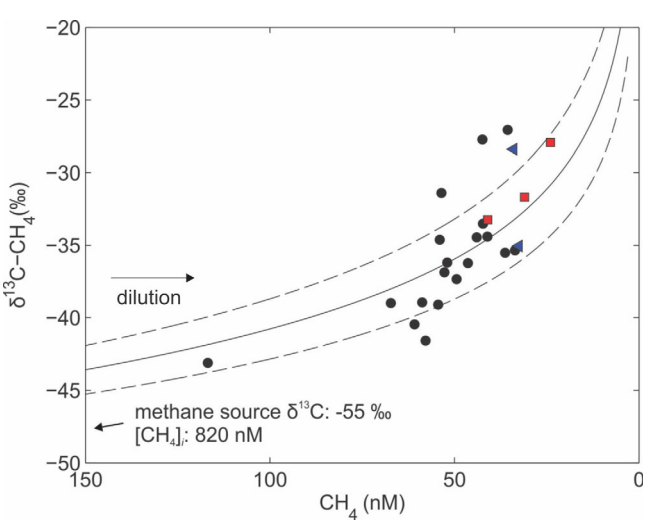

Figure 6. Carbon isotope signature of dissolved methane in bottom water (lower 150 m) near the MASOX site (Figure 1): within the modeled box volume (black circles), in overlying water (red squares), and bottom water >2 km from the seafloor seeps (blue triangles). Black lines are Rayleigh distillation curves for the average isotopic fractionation factor (solid) with $\pm 2\sigma$ uncertainty (dashed). Scatter of data about the Rayleigh distillation curve is due to variable seep methane fluxes as well as methane oxidation rates [*Steinle et al.*, 2015].

The stable carbon isotope composition of methane in bottom waters (lower 150 m) near the MASOX site also supports extensive methane oxidation. All measured stable isotopic signatures of dissolved methane were considerably higher than the reported composition of the released gas ($-55‰$ [*Sahling et al.*, 2014]). The light carbon isotope (^{12}C) is oxidized in preference to ^{13}C, leaving the remaining methane pool isotopically heavy (Figure 6). Assuming a closed system, the stable isotopic composition (δ^{13}C-CH$_4$) can be described according to the Rayleigh distillation model:

$$\delta^{13}\text{C-CH}_4 = 1000 \cdot (1/\alpha - 1) \cdot ln\left([\text{CH}_4]/[\text{CH}_4]_i\right) + (\delta^{13}\text{C-CH}_4)_i \quad (7)$$

where α is the carbon isotope fractionation factor for aerobic methane

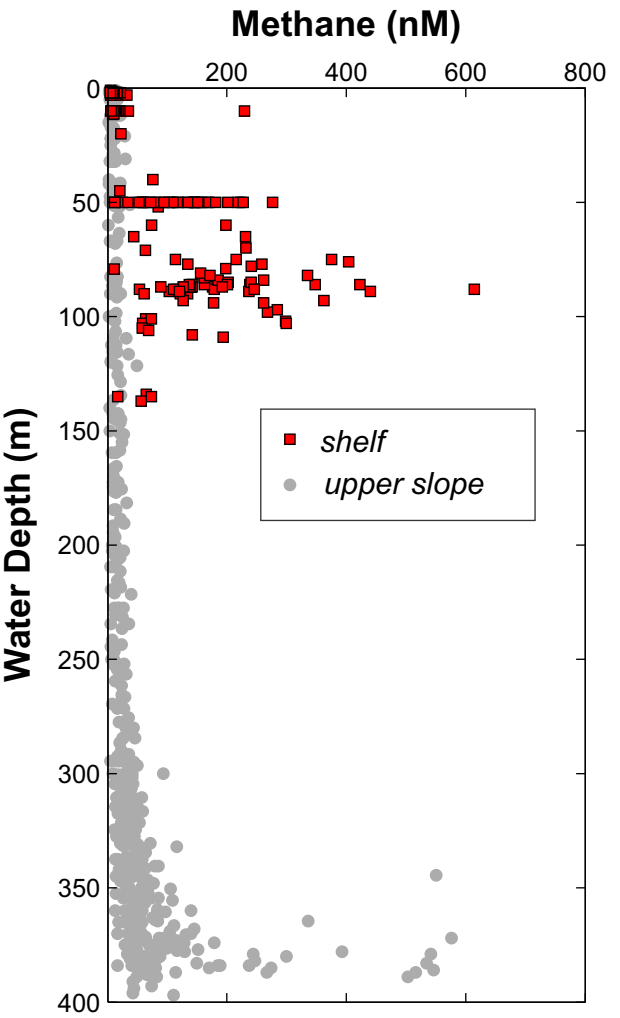

Figure 7. Variation in dissolved methane concentration with depth over the shelf region (80–150 m water depth; red squares) and on the upper slope near the landward limit of the GHSZ (380–400 m water depth; circles).

oxidation, $[CH_4]$ is the dissolved methane concentration, and subscript *i* indicates the initial methane concentration or isotope signature [*Coleman et al.*, 1981]. Given the very low methane background concentration in open ocean North Atlantic Waters of less than 1 nM [*Rehder et al.*, 1999], dilution can be expected to reduce $[CH_4]$ without significantly changing δ^{13}C-CH_4. Taking the highest measured methane concentration (820 nM) and the average δ^{13}C-CH_4 value of bubbles released at the seafloor ($-55‰$ [*Sahling et al.*, 2014]) as initial conditions and solving for α yields an average isotopic fractionation factor of 1.007 ± 0.001 (standard deviation), which is consistent with previous work in this area ($\alpha = 1.008$) [*Damm et al.*, 2005] and within the range previously reported for the marine environment ($\alpha = 1.002$ to 1.035) [*Grant and Whiticar*, 2002]. If $\alpha = 1.007$, equation (7) indicates that ~2–18% of the methane from the seafloor seeps is oxidized prior to advection away from the seep site.

The model only describes the fate of methane released at the seafloor which dissolves in the lower part of the water column; the effects of continued methane supply are not included. As bottom water currents in this area are fast, the methane released at the seafloor is rapidly flushed away from its source in the northward-flowing WSC. Monthly mean current velocity in the WSC offshore western Svalbard is up to ~24 cm s^{-1} on the upper continental slope [*Fahrbach et al.*, 2001; *Schauer et al.*, 2004], with wintertime peaks exceeding 50 cm s^{-1}. The net effects of tidal displacement are expected to be minor, as neither methane concentrations nor other bottom water properties were related to the tidal phase during sampling.

A volume of water moving with currents at 24 cm s^{-1} would pass over the seepage region in approximately 0.6 days. During this time, the total input of methane at the seafloor from seep bubbles is estimated to be ~10 mol (assuming a bubble seep methane flux of 16 mol d^{-1} m^{-1} [*Sahling et al.*, 2014]). For this input flux, the accumulated dissolved methane concentration in the box is 50–700 nM, in good agreement with measured concentrations. Thus, our model of methane loss is consistent with both our observations and measurements of methane fluxes across the seabed. Within the time required for half of the methane released at the seafloor to be consumed by oxidation and lost by mixing, advection in the WSC can be expected to transport the modeled parcel of high-methane bottom water northward from the seepage site to a latitude of >80°N, where the WSC flows over the Yermak Plateau and is partially recirculated through the Fram Strait [*Gascard et al.*, 1995]. Although this water will still contain methane sourced from the seepage region, the pattern of circulation in this region implies that it remains at depth and is not expected to come into contact with the atmosphere [*Elliott et al.*, 2011].

Table 2. Sea to Air Methane Fluxes and Associated Parameters

		Surface Seawater CH_4 Concentration (nM)	Temperature (°C)	Salinity	Atmospheric Pressure (mbar)	Atmospheric CH_4 Mole Fraction (ppb)	Percent Saturation (%)	Wind Speed (u_{10}) (m s^{-1})	Sea → Air Flux (mmol m^{-2} d^{-1})
Equilibrator System									
Main study area	Average	4.7	5.4	34	1007		145	7	4
	Minimum	3.1	4.4	33	1016		100	0	0
	Maximum	6.4	8.5	35	990		191	17	17
Offshore	Average	3.4	6.7	34	1004		111	8	1
	Minimum	3.1	5.3	33	1012		100	2	0
	Maximum	5.9	9.6	34	994		187	13	10
North	Average	4.2	8.4	34	1013		139	4	1
	Minimum	3.2	4.8	33	1014		107	0	0
	Maximum	5.7	9.7	34	1012		173	8	4
South	Average	4.4	5.9	34	9936		139	8	3
	Minimum	3.1	4.1	33	1002		101	3	0
	Maximum	6.9	7.2	34	9913		210	17	18
Outer shelf	Average	5.0	5.1	33	1006		154	9	6
	Minimum	3.2	4.2	32	1017		101	4	0
	Maximum	6.9	7.0	34	9871		212	17	25
Inner shelf	Average	8.5	4.6	33	1001		258	7	8
	Minimum	4.4	3.7	32	1012		138	0	0
	Maximum	52	5.5	34	9866		1579	14	36
Depth Profiles									
2012	Average	11	5.0	34	999	1891	336	9	30
	Minimum	4.5	4.8	34	989	1883	136	3	15
	Maximum	17	7.0	35	1005	1899	572	17	45
2011	Average	8.9	5.0	33	1014	1866	271	8	16
	Minimum	2.9	3.4	29	989	1852	81	0	8
	Maximum	9.0	6.5	35	1023	1890	298	18	32

4.2.2. Sources of Methane to the Upper Water Column

The complete dissolution of methane bubbles below 200 m water depth precludes direct input of methane to the upper water column by bubble transport. Slow diapycnal mixing rates coupled with high bottom water current speeds also mean that the seafloor seeps cannot contribute significant dissolved methane to surface waters directly above seep sites under the observed summer conditions. However, elevated methane concentrations are found in both intermediate (depth < 200 m, $\sigma_\theta > 27.5$ kg m^{-3}) and surface ($\sigma_\theta < 27.5$ kg m^{-3}) waters. Potential alternative sources of methane to the upper part of the water column include: (i) isopycnal mixing of methane from seafloor seeps located on the shelf, (ii) diapycnal mixing of methane from upstream seafloor seeps to the south of the study area, and (iii) production of methane in near-surface waters.

Seafloor methane seepage also occurs on the shallow (<100 m) continental shelf offshore Svalbard approximately 15 km east of the landward limit of the GHSZ [*Sahling et al.*, 2014]. Because the water depth is shallow, larger methane bubbles can rise all the way through the water column and methane concentrations are high even in surface waters, establishing a large concentration gradient between shelf and upper slope waters (Figure 7). Cold Arctic ESC water on the shelf is separated from warm Atlantic WSC water on the upper slope by a strong density-compensated halocline (the Arctic Front) [e.g., *Cottier and Venables*, 2007; *Saloranta and Svendsen*, 2001], which allows offshore isopycnal mixing of methane from the shelf with the upper water column at the GHSZ limit. Mechanisms for enhanced isopycnal turbulent diffusion across the Arctic Front include barotropic instability due to the difference in current speed between WSC and ESC waters [*Saloranta and Svendsen*, 2001; *Teigen et al.*, 2010] and interleaving and cabbeling: isopycnal mixing of water with different salinity and temperature to produce parcels of denser water which then sink, generating vertical mixing [*Cottier and Venables*, 2007]. It has also been shown that meandering of the warm core of the WSC onto and away from the study site causes variable entrainment of ESC waters over the upper slope [*Steinle et al.*, 2015].

WSC water flowing northward into the study area may carry dissolved methane from upstream sources to the south. Slow upward diapycnal transport of methane from bottom water into intermediate-depth waters is likely to occur during transport. While the recent discovery of extensive seafloor methane seeps aligned along the

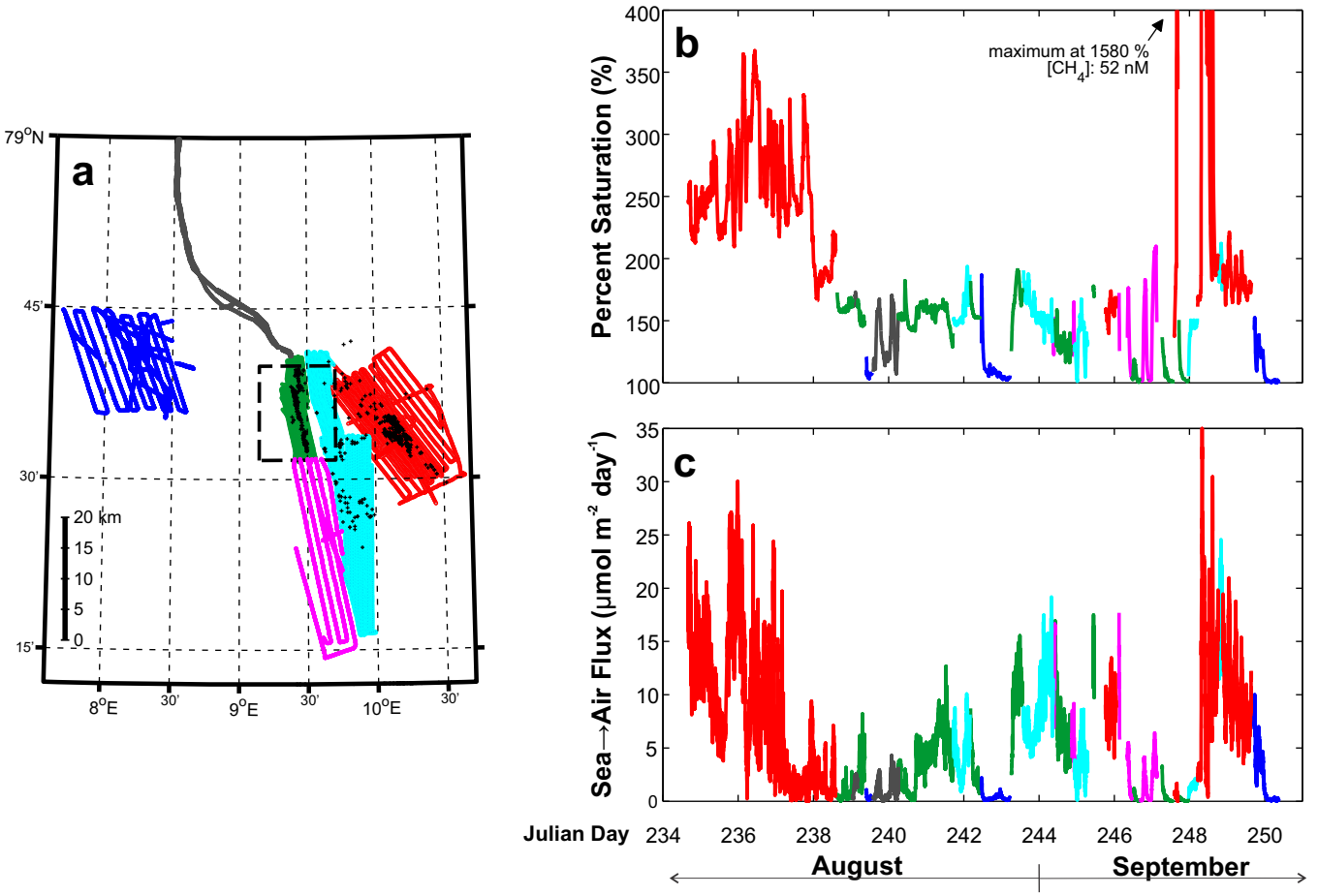

Figure 8. (a) Region surveyed using the equilibrator system. Colors indicate different regions described in Table 2: purple = south, green = main study area, light blue = outer shelf, dark blue = offshore, red = inner shelf, grey = north. Black crosses indicate positions of methane seeps, and black dashed rectangle indicates the extent of the map shown in Figures 4 and 1b. (b) Equilibrator data expressed as methane saturation with respect to atmospheric equilibrium, and (c) sea-air methane flux for each region.

landward limit of hydrate stability offshore North America [*Skarke et al.*, 2014] supports the idea that the location of seafloor methane seeps is regulated by hydrate dissociation, extensive acoustic surveys offshore western Svalbard have found no evidence for southward extension of seepage along the landward limit of the GHSZ up to 20 km to the south of the study area [*Sahling et al.*, 2014]. However, a single depth profile ~30 km to the south of our study area revealed methane concentrations increasing with depth to a bottom water maximum of 40 nM (supporting information Figure S3), and elevated methane concentrations in water on the upper slope ~150 km south of our study area have previously been reported [*Damm et al.*, 2005]. This suggests that seafloor methane seeps are likely to exist to the south, but these seeps are apparently patchy and/or temporally variable, and may not occur at the limit of hydrate stability. More extensive echo sounder surveys and water column measurements are needed to appropriately quantify any contribution of methane sources to the south of our study area.

Table 3. Sea to Air Methane Fluxes[a]

Location	Water Depth (m)	Diffusive Flux (μmol m^{-2} d^{-1})	Reference
Upper slope offshore western Svalbard	~400	20 (8–45)	This study, Niskin bottle samples
		4 (0–17)	This study, equilibrator system
Shelf offshore western Svalbard	~100	8 (0–36)	This study, equilibrator system.
East Siberian Arctic Sea	<60	230 (190–300)[b]	*Shakhova et al.* [2010b]
Open Arctic Ocean north of Alaska	~3500	125 (30–500)	*Kort et al.* [2012]
Atlantic Ocean:			
Open ocean		0.2	*Rhee et al.* [2009]
Coastal regions		2	

[a]Values in brackets are minimum and maximum fluxes.
[b]Corrected for differences in the choice of gas transfer coefficient (*k*).

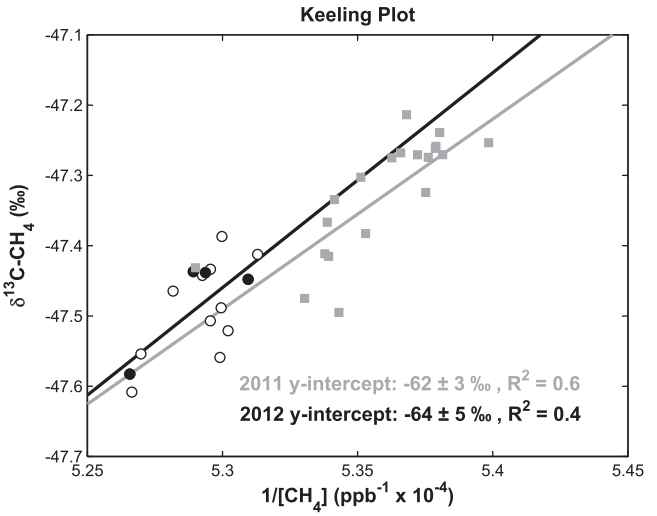

Figure 9. Keeling plot of atmospheric methane mole fraction versus δ^{13}C-CH_4: 2011 data (grey squares) were all collected within 3 km of seafloor methane seeps, 2012 data were collected within 5 km of seeps (filled circles), and within >5 km and <50 km from the seeps (open circles).

Production of methane within the upper water column is well documented throughout the world's oceans [e.g., *Damm et al*., 2010; *Karl and Tilbrook*, 1994; *Sasakawa et al*., 2008; *Scranton and Brewer*, 1977] with concentrations exceeding atmospheric equilibrium (~3 nM) often observed at the depth of the pycnocline [*Reeburgh*, 2007]. Dissolved methane concentrations of up to 55 nM in surface waters on the shelf to the south of Spitsbergen (Storfjorden) have been attributed to in situ methanogenesis [*Damm et al*., 2008]. In this setting, methane is able to accumulate because oxidation is slow and waters are strongly stratified, preventing exchange with the atmosphere. Several, but not all, of our methane depth profiles collected at the GHSZ limit (~400 m water depth) show higher dissolved methane concentrations (up to ~25 nM) close to the pycnocline. However, our 2012 survey reveals that low-salinity surface waters are intermittently absent (Figure 3b), preventing the development of a permanent pycnocline. An alternative explanation for accumulation of dissolved methane at the pycnocline is that methane rising from the seafloor seeps pools beneath the density barrier [*Solomon et al*., 2009].

4.2.3. Methane Flux to the Atmosphere

Sea to air methane fluxes calculated from measured surface water methane concentrations in both Niskin bottle samples and by the equilibrator system are given in Table 2 and their spatial variation is shown in Figure 8. Flux calculations using boundary layer models [e.g., *Liss and Slater*, 1974; *Wanninkhof et al*., 2009] are determined by the concentration gradient between surface waters and the atmosphere, and the gas transfer velocity which is mainly parameterized by wind speed. Atmospheric methane mole fractions were relatively stable in the area during sampling, and variability in methane solubility with surface seawater temperature and salinity is negligible for the observed range of conditions. Surface seawater methane supersaturation (Figure 8b) therefore predominantly reflects changes in surface seawater methane concentrations (Figure 4), while sea-air fluxes (Figure 8c) incorporate wind speed effects on gas transfer velocities.

Both methane saturation and sea to air methane fluxes were highest on the shelf, where the water depth is relatively shallow. Fewer seafloor seeps are present on the outer part of the shelf and water depths become progressively deeper, so that methane fluxes are lower and similar to those calculated at the landward limit of the GHSZ. Lowest methane fluxes were found furthest offshore. High methane concentrations in surface waters along the 400 m bathymetric contour to the north of the main study site suggest that methane transported at depth in the WSC from the seeps at the limit of the GHSZ may mix vertically during northward advection and reach surface waters downstream. Enhanced vertical mixing is suggested by wintertime WSC heat loss studies, which show that mass exchange between the upper 10–20 m of the water column and the stratified interior occurs on time scales faster than one day [*Boyd and D'Asaro*, 1994].

Table 3 compares fluxes of methane from the upper slope and shelf region offshore Svalbard to the atmosphere with other sources of atmospheric methane in the Arctic and elsewhere. The source strength of the Svalbard seeps is 1–2 orders of magnitude lower than that reported for the East Siberian Arctic (ESA) Sea, where methane (likely derived from thawing permafrost) is ejected from the seafloor at very shallow water depths (<60 m) [*Shakhova et al*., 2014, 2010b]. The fluxes that we measure are also lower than those observed during an aircraft survey over open leads (fractures in sea ice) and regions with fractional ice cover in the Arctic Ocean [*Kort et al*., 2012], which are attributed to release of methane that may accumulate under ice in the winter months [*Shakhova et al*., 2010a] and/or biological production of methane in the vicinity of melting ice [*He et al*., 2013].

In support of the relatively low sea to air flux, atmospheric methane mole fractions above our study region are not significantly higher than those measured 5 to >50 km from the seafloor seeps. Keeling plots of the $\delta^{13}C$ signature of atmospheric methane (Figure 9) indicate that the overall $\delta^{13}C\text{-}CH_4$ signature of the methane sources to this area between $-62 \pm 3‰$ (2011) and $-64 \pm 5‰$ (2012). These values suggest that biogenic sources such as high-latitude wetlands, with $\delta^{13}C\text{-}CH_4 < -65‰$ [*Sriskantharajah et al*., 2012], are the main source of atmospheric methane, but they do not preclude some (albeit small) contribution from seafloor methane seeps, which have $\delta^{13}C\text{-}CH_4 \sim -55‰$ [*Fisher et al*., 2011; *Sahling et al*., 2014].

5. Summary and Conclusions

Dissolution of methane from seafloor bubble seeps at the landward limit of gas hydrate stability offshore western Svalbard leads to high concentrations of dissolved methane (up to 825 nM) in bottom waters of the northward-flowing West Spitsbergen Current. Methane concentrations in upper and intermediate waters are lower (2–50 nM), but nevertheless supersaturated with respect to the atmosphere resulting in methane transfer across the sea-air interface. Simple box modeling indicates that methane released at the seafloor is mainly lost by oxidation (to carbon dioxide) and advection by fast bottom water currents. Thus, relatively high concentrations of methane in intermediate and surface waters cannot be attributed to seafloor seepage at the landward limit of gas hydrate stability; rather, the most likely source of this methane is entrainment and isopycnal mixing with waters from the shelf, which have high methane contents as a result of seafloor seepage on the shelf itself. High concentrations of methane at the sea surface to the north of the seafloor seeps suggest that enhanced vertical mixing of methane from the WSC may provide a mechanism for methane escape from seafloor seeps at the GHSZ limit to the atmosphere on longer time scales.

Although surface waters are supersaturated with methane throughout our study area, the sea-air methane flux is relatively small. In support of this, measurements of atmospheric methane mole fractions and carbon isotopic composition reveal neither high mole fractions close to the seafloor methane seeps, nor relatively heavy isotopic signatures consistent with gas bubbles in the water column. Thus, aerobic methanotrophy in the water column at the GHSZ limit offshore western Svalbard provides an effective barrier to direct release of significant quantities of methane, including that which may be released from methane hydrate, to the atmosphere.

Acknowledgments

All water column methane concentration and oxidation rate data from MSM21/4 are available from the PANGAEA data library: http://doi.pangaea.de/10.1594/PANGAEA.844013, and methane isotope data are provided in supporting information Table S8. Water column methane concentration data for JR253 are available from the British Oceanographic Data Centre (BODC: http://www.bodc.ac.uk/). Atmospheric methane data are provided in supporting information Table S9. Data from He387 can be requested from Gregor Rehder (gregor.rehder@io-warnemuende.de), and will be transferred to the MEMENTO database (https://memento.geomar.de [*Bange et al*., 2009]) by the end of 2015. We thank Captain M. Burgan of the RRS James Clark Ross, Captain K. Bergmann of the R/V Maria S. Merian, and shipboard scientific parties, officers, and crews of cruises JR253, MSM21/4, and He-387. M. Glockzin (IOW) is acknowledged for the operation and maintenance of the CH_4 equilibration system used on He387. Kerstin Kretschmer is acknowledged for technical support for water sampling during MSM 21/4 and Catherine Cole and Belinda Alker for assistance in sampling during JR253. This project was funded by a UK Natural Environment Research Council (NERC) National Capability programme and NERC grant NE/D005728/2, and was part of a PhD study funded by the Graduate School of Ocean and Earth Science (University of Southampton, UK) and Natural Sciences and Engineering Research Council of Canada Postgraduate Scholarships awarded to C.A.G. (PGS-M and PGS-D3). Funding for R/V Heincke cruise 387 was provided by MARUM-Center for Marine Environmental Studies. The NERC Life Sciences Mass Spectrometry Steering Committee awarded a "grant in kind" for analytical support. Further support for collaboration was provided through the EU COST Action PERGAMON (ESSEM 0902) and through a D-A-CH project funded by the Swiss National Science Foundation and German Research Foundation (grant 200021L 138057) and the Cluster of Excellence "The Future Ocean" funded by the German Research Foundation.

References

Aagaard, K., A. Foldvik, and S. R. Hillman (1987), The West Spitsbergen Current: Disposition and water mass transformation, *J. Geophys. Res.*, *92*(C4), 3778–3784, doi:10.1029/JC092iC04p03778.

Bange, H. W., T. G. Bell, M. Cornejo, A. Freing, G. Uher, R. C. Upstill-Goddard, and G. Zhang (2009), MEMENTO: A proposal to develop a database of marine nitrous oxide and methane measurements, *Environ. Chem.*, *6*, 195–197, doi:10.1071/EN09033.

Berndt, C., et al. (2014), Temporal constraints on hydrate-controlled methane seepage off Svalbard, *Science*, *343*(6168), 284–287, doi:10.1126/science.1246298.

Biastoch, A., et al. (2011), Rising Arctic Ocean temperatures cause gas hydrate destabilization and ocean acidification, *Geophys. Res. Lett.*, *38*, L08602, doi:10.1029/2011GL047222.

Boetius, A., and F. Wenzhöfer (2013), Seafloor oxygen consumption fuelled by methane from cold seeps, *Nat. Geosci.*, *6*, 725–734, doi:10.1038/ngeo1926.

Boyd, T. J., and E. A. D'Asaro (1994), Cooling of the West Spitsbergen Current: Wintertime observations west of Svalbard, *J. Geophys. Res.*, *99*(C11), 22,597–22,618, doi:10.1029/94JC01824.

Coleman, D. D., J. B. Risatti, and M. Schoell (1981), Fractionation of carbon and hydrogen isotopes by methane-oxidizing bacteria, *Geochim. Cosmochim. Acta*, *45*, 1033–1037, doi:10.1016/0016-7037(81)90129-0.

Cottier, F. R., and E. J. Venables (2007), On the double-diffusive and cabbeling environment of the Arctic Front, West Spitsbergen, *Polar Res.*, *26*(2), 152–159, doi:10.1111/j.1751-8369.2007.00024.x.

Damm, E., A. Mackensen, G. Budéus, E. Faber, and C. Hanfland (2005), Pathways of methane in seawater: Plume spreading in an Arctic shelf environment (SW-Spitsbergen), *Cont. Shelf Res.*, *25*(12-13), 1453–1472, doi:10.1016/j.csr.2005.03.003.

Damm, E., R. P. Kiene, J. Schwarz, E. Falck, and G. Dieckmann (2008), Methane cycling in Arctic shelf water and its relationship with phytoplankton biomass and DMSP, *Mar. Chem.*, *109*(1-2), 45–59, doi:10.1016/j.marchem.2007.12.003.

Damm, E., E. Helmke, S. Thoms, U. Schauer, E. Nöthig, K. Bakker, and R. P. Kiene (2010), Methane production in aerobic oligotrophic surface water in the central Arctic Ocean, *Biogeosciences*, *7*, 1099–1108, doi:10.5194/bg-7-1099-2010.

Deng, Z., T. Yu, S. Shi, J. Jin, and K. Wu (2014), The global distribution of diapycnal mixing and mixing coefficient tensor in the upper 2000 m ocean from Argo observations, *Mar. Geod.*, *37*(3), 337–353, doi:10.1080/01490419.2013.873099.

Dickens, G. R. (2011), Down the rabbit hole: Toward appropriate discussion of methane release from gas hydrate systems during the Paleocene-Eocene thermal maximum and other past hyperthermal events, *Clim. Past*, *7*(3), 831–846, doi:10.5194/cp-7-831-2011.

Elliott, S., M. Maltrud, M. Reagan, G. Moridis, and P. Cameron-Smith (2011), Marine methane cycle simulations for the period of early global warming, *J. Geophys. Res.*, *116*, G01010, doi:10.1029/2010JG001300.

Fahrbach, E., J. Meincke, S. Østerhus, G. Rohardt, J. Schauer, V. Tverberg, and J. Verduin (2001), Direct measurements of volume transports through Fram Strait, *Polar Res.*, *20*(2), 217–224, doi:10.1111/j.1751-8369.2001.tb00059.x.

Ferré, B., J. Mienert, and T. Feseker (2012), Ocean temperature variability for the past 60 years on the Norwegian-Svalbard margin influences gas hydrate stability on human time scales, *J. Geophys. Res.*, *117*, C10017, doi:10.1029/2012JC008300.

Fisher, R. E., D. Lowry, O. Wilkin, S. Sriskantharajah, and E. G. Nisbet (2006), High-precision, automated stable isotope analysis of atmospheric methane and carbon dioxide using continuous-flow isotope-ratio mass spectrometry, *Rapid Commun. Mass Spectrom.*, *20*(2), 200–208, doi:10.1002/rcm.2300.

Fisher, R. E., et al. (2011), Arctic methane sources: Isotopic evidence for atmospheric inputs, *Geophys. Res. Lett.*, *38*, L21803, doi:10.1029/2011GL049319.

Gascard, J.-C., C. Richez, and C. Rouault (1995), New insights on large-scale oceanography in Fram Strait: The West Spitsbergen Current, in *Arctic Oceanography: Marginal Ice Zones and Continental Shelves*, edited by W. O. Smith and J. M. Grebmeir, pp. 131–182, AGU, Washington, D. C., doi:10.1029/CE049p0131.

Gentz, T., E. Damm, J. Schneider von Deimling, S. Mau, D. F. McGinnis, and M. Schlüter (2014), A water column study of methane around gas flares located at the West Spitsbergen continental margin, *Cont. Shelf Res.*, *72*, 107–118, doi:10.1016/j.csr.2013.07.013.

Grant, N. J., and M. J. Whiticar (2002), Stable carbon isotopic evidence for methane oxidation in plumes above Hydrate Ridge, Cascadia Oregon Margin, *Global Biogeochem. Cycles*, *16*(4), 1124, doi:10.1029/2001GB001851.

Gülzow, W., G. Rehder, B. Schneider, J. Schneider von Deimling, and B. Sadkowiak (2011), A new method for continuous measurement of methane and carbon dioxide in surface waters using off-axis integrated cavity output spectroscopy (ICOS): An example from the Baltic Sea, *Limnol. Oceanogr. Methods*, *9*(5), 176–184, doi:10.4319/lom.2011.9.176.

Hanson, R. S., and T. E. Hanson (1996), Methanotrophic bacteria, *Microbiol. Rev.*, *60*(2), 439–471.

He, X., L. Sun, Z. Xie, W. Huang, N. Long, Z. Li, and G. Xing (2013), Sea ice in the Arctic Ocean: Role of shielding and consumption of methane, *Atmos. Environ.*, *67*, 8–13, doi:10.1016/j.atmosenv.2012.10.029.

Hsu, S. A., E. A. Meindl, and D. B. Gilhousen (1994), Determining the power-law wind-profile exponent under near-neutral stability conditions at sea, *J. Appl. Meteorol.*, *33*(6), 757–765.

Hu, L., S. A. Yvon-Lewis, J. D. Kessler, and I. R. MacDonald (2012), Methane fluxes to the atmosphere from deepwater hydrocarbon seeps in the northern Gulf of Mexico, *J. Geophys. Res.*, *117*, C01009, doi:10.1029/2011JC007208.

Intergovernmental Panel on Climate Change (2013), *Climate Change 2013: The Physical Science Basis, Contribution of Working Group I to the Fourth Assessment Report of the Intergovernmental Panel on Climate Change*, edited by T. F. Stocker et al., Cambridge Univ. Press, Cambridge, U. K., doi:10.1017/CBO9781107415324.

Judd, A., and M. Hovland (2007), *Seabed Fluid Flow: The Impact on Geology, Biology and the Marine Environment*, 475 pp., Cambridge Univ. Press, Cambridge, U. K., doi:10.1017/CBO9780511535918.

Karl, D. M., and B. D. Tilbrook (1994), Production and transport of methane in oceanic particulate organic matter, *Nature*, *368*, 732–734, doi:10.1038/368732a0.

Kirschke, S., et al. (2013), Three decades of global methane sources and sinks, *Nat. Geosci.*, *6*, 813–823, doi:10.1038/ngeo1955.

Knies, J., E. Damm, J. Gutt, U. Mann, and L. Pinturier (2004), Near-surface hydrocarbon anomalies in shelf sediments off Spitsbergen: Evidences for past seepages, *Geochem. Geophys. Geosyst.*, *5*, Q06003, doi:10.1029/2003GC000687.

Kort, E. A., et al. (2012), Atmospheric observations of Arctic Ocean methane emissions up to 82° north, *Nat. Geosci.*, *5*, 318–321, doi:10.1038/ngeo1452.

Krey, V., et al. (2009), Gas hydrates: Entrance to a methane age or climate threat?, *Environ. Res. Lett.*, *4*, 034007, doi:10.1088/1748-9326/4/3/034007.

Largier, J. L. (2003), Considerations in estimating larval dispersal distances from oceanographic data, *Ecol. Appl.*, *13*(1), S71–S89, doi:10.1038/35003164.

Ledwell, J. R., A. J. Watson, and C. S. Law (1993), Evidence for slow mixing accross the pycnocline from and open-ocean tracer-release experiment, *Nature*, *364*, 701–703, doi:10.1038/364701a0.

Ledwell, J. R., A. J. Watson, and C. S. Law (1998), Mixing of a tracer in the pycnocline, *J. Geophys. Res.*, *103*(C10), 21,499–21,529, doi:10.1029/98JC01738.

Ledwell, J. R., E. T. Montgomery, K. L. Polzin, L. C. St. Laurent, R. W. Schmitt, and J. M. Toole (2000), Evidence for enhanced mixing over rough topography in the abyssal ocean, *Nature*, *403*, 179–182, doi:10.1038/35003164.

Leifer, I., and R. K. Patro (2002), The bubble mechanism for methane transport from the shallow sea bed to the surface: A review and sensitivity study, *Cont. Shelf Res.*, *22*(16), 2409–2428, doi:10.1016/S0278-4343(02)00065-1.

Liss, P. S., and L. Merlivat (1986), Air-sea gas exchange rates: Introduction and synthesis, in *The Role of Air-Sea Exchange in Geochemical Cycling*, edited by P. Buat-Ménard, pp. 113–129, Springer, Dordrecht, Netherlands, doi:10.1007/978-94-009-4738-2_5.

Liss, P. S., and P. G. Slater (1974), Flux of gases across the air-sea interface, *Nature*, *247*, 181–184, doi:10.1038/247181a0.

Mau, S., M. B. Heintz, and D. L. Valentine (2012), Quantification of CH_4 loss and transport in dissolved plumes of the Santa Barbara Channel, California, *Cont. Shelf Res.*, *32*, 110–120, doi:10.1016/j.csr.2011.10.016.

Mau, S., J. Blees, E. Helmke, H. Niemann, and E. Damm (2013), Vertical distribution of methane oxidation and methanotrophic response to elevated methane concentrations in stratified waters of the Arctic fjord Storfjorden (Svalbard, Norway), *Biogeosciences*, *10*(10), 6267–6278, doi:10.5194/bg-10-6267-2013.

McGillis, W. R., J. B. Edson, J. D. Ware, J. W. H. Dacey, J. E. Hare, C. W. Fairall, and R. Wannikhof (2001), Carbon dioxide flux techniques performed during GasEx-98, *Mar. Chem.*, *75*, 267–280, doi:10.1016/S0304-4203(01)00042-1.

McGinnis, D. F., J. Greinert, Y. Artemov, S. E. Beaubien, and A. Wüest (2006), Fate of rising methane bubbles in stratified waters: How much methane reaches the atmosphere?, *J. Geophys. Res.*, *111*, C09007, doi:10.1029/2005JC003183.

Milkov, A. V. (2004), Global estimates of hydrate-bound gas in marine sediments: How much is really out there?, *Earth Sci. Rev.*, *66*(3-4), 183–197, doi:10.1016/j.earscirev.2003.11.002.

Naudts, L., J. Greinert, Y. Artemov, P. Staelens, J. Poort, P. Van Rensbergen, and M. De Batist (2006), Geological and morphological setting of 2778 methane seeps in the Dnepr paleo-delta, northwestern Black Sea, *Mar. Geol.*, *227*(3-4), 177–199, doi:10.1016/j.margeo.2005.10.005.

Niemann, H., L. Steinle, J. Blees, I. Bussmann, T. Treude, S. Krause, M. Elvert, and M. F. Lehmann (2015), Toxic effects of lab-grade butyl rubber stoppers on aerobic methane oxidation, *Limnol. Oceanogr. Methods*, *13*(1), 40–52, doi:10.1002/lom3.10005.

Nightingale, P. D., G. Malin, C. S. Law, A. J. Watson, P. S. Liss, M. I. Liddicoat, J. Boutin, and R. C. Upstill-Goddard (2000), In situ evaluation of air-sea gas exchange parameterizations using novel conservative and volatile tracers, *Global Biogeochem. Cycles*, *14*(1), 373–387, doi:10.1029/1999GB900091.

Padman, L., and T. M. Dillon (1991), Turbulent mixing near the Yermak Plateau during the Coordinated Eastern Arctic Experiment, *J. Geophys. Res.*, *96*(C3), 4769–4782, doi:10.1029/90JC02260.

Reagan, M. T., and G. J. Moridis (2009), Large-scale simulation of methane hydrate dissociation along the West Spitsbergen Margin, *Geophys. Res. Lett.*, *36*, L23612, doi:10.1029/2009GL041332.
Reeburgh, W. S. (2007), Oceanic methane biogeochemistry, *Chem. Rev.*, *107*(2), 486–513, doi:10.1021/cr050362v.
Rehder, G., R. S. Keir, E. Suess, and M. Rhein (1999), Methane in the northern Atlantic controlled by microbial oxidation and atmospheric history, *Geophys. Res. Lett.*, *26*(5), 587–590.
Rehder, G., I. Leifer, P. G. Brewer, G. Friederich, and E. T. Peltzer (2009), Controls on methane bubble dissolution inside and outside the hydrate stability field from open ocean field experiments and numerical modeling, *Mar. Chem.*, *114*(1–2), 19–30, doi:10.1016/j.marchem.2009.03.004.
Rhee, T. S., A. J. Kettle, and M. O. Andreae (2009), Methane and nitrous oxide emissions from the ocean: A reassessment using basin-wide observations in the Atlantic, *J. Geophys. Res.*, *114*, D12304, doi:10.1029/2008JD011662.
Rippeth, T. P., B. J. Lincoln, Y.-D. Lenn, J. A. M. Green, A. Sundfjord, and S. Bacon (2015), Tide-mediated warming of Arctic halocline by Atlantic heat fluxes over rough topography, *Nat. Geosci.*, *8*(3), 191–194, doi:10.1038/ngeo2350.
Römer, M., et al. (2014), First evidence of widespread active methane seepage in the Southern Ocean, off the sub-Antarctic island of South Georgia, *Earth Planet. Sci. Lett.*, *403*, 166–177, doi:10.1016/j.epsl.2014.06.036.
Sahling, H., et al. (2012), *R/V Heincke Cruise Report HE-387. Gas Emissions at the Svalbard Continental Margin. Longyearbyen-Bremerhaven 20 August – 16 September 2012*, *No. 291*, 170 pp., Berichte, MARUM—Zentrum für Mar. Umweltwissenschaften, Fachbereich Geowissenschaften, Univ. Bremen, Bremen, Germany.
Sahling, H., et al. (2014), Gas emissions at the continental margin west of Svalbard: Mapping, sampling, and quantification, *Biogeosciences*, *11*, 6029–6046, doi:10.5194/bgd-11-7189-2014.
Saloranta, T. M., and P. M. Haugan (2004), Northward cooling and freshening of the warm core of the West Spitsbergen Current, *Polar Res.*, *23*(1), 79–88, doi:10.1111/j.1751-8369.2004.tb00131.x.
Saloranta, T. M., and H. Svendsen (2001), Across the Arctic front west of Spitsbergen: High-resolution CTD sections from 1998-2000, *Polar Res.*, *20*(2), 177–184, doi:10.1111/j.1751-8369.2001.tb00054.x.
Sasakawa, M., U. Tsunogai, S. Kameyama, F. Nakagawa, Y. Nojiri, and A. Tsuda (2008), Carbon isotopic characterization for the origin of excess methane in subsurface seawater, *J. Geophys. Res.*, *113*, C03012, doi:10.1029/2007JC004217.
Schauer, U., E. Fahrbach, S. Osterhus, and G. Rohardt (2004), Arctic warming through the Fram Strait: Oceanic heat transport from 3 years of measurements, *J. Geophys. Res.*, *109*, C06026, doi:10.1029/2003JC001823.
Schmale, O., M. Haeckel, and D. F. McGinnis (2011), Response of the Black Sea methane budget to massive short-term submarine inputs of methane, *Biogeosciences*, *8*(4), 911–918, doi:10.5194/bg-8-911-2011.
Schneider von Deimling, J., G. Rehder, J. Greinert, D. F. McGinnis, A. Boetius, and P. Linke (2011), Quantification of seep-related methane gas emissions at Tommeliten, North Sea, *Cont. Shelf Res.*, *31*(7–8), 867–878, doi:10.1016/j.csr.2011.02.012.
Scranton, M. I., and P. G. Brewer (1977), Occurrence of methane in the near-surface waters of the western subtropical North-Atlantic, *Deep Sea Res.*, *24*(2), 127–138, doi:10.1016/0146-6291(77)90548-3.
Shakhova, N., I. Semiletov, I. Leifer, A. Salyuk, P. Rekant, and D. Kosmach (2010a), Geochemical and geophysical evidence of methane release over the East Siberian Arctic Shelf, *J. Geophys. Res.*, *115*, C08007, doi:10.1029/2009JC005602.
Shakhova, N., I. Semiletov, A. Salyuk, V. Yusupov, D. Kosmach, and Ö. Gustafsson (2010b), Extensive methane venting to the atmosphere from sediments of the East Siberian Arctic Shelf, *Science*, *327*(5970), 1246–1250, doi:10.1126/science.1182221.
Shakhova, N., et al. (2014), Ebullition and storm-induced methane release from the East Siberian Arctic Shelf, *Nat. Geosci.*, *7*, 64–70, doi:10.1038/ngeo2007.
Shaw, W. J., and T. P. Stanton (2014), Vertical diffusivity of the Western Arctic Ocean halocline, *J. Geophys. Res. Oceans*, *119*, 5017–5038, doi:10.1002/2013JC009598.
Skarke, A., C. Ruppel, M. Kodis, D. Brothers, and E. Lobecker (2014), Widespread methane leakage from the sea floor on the northern US Atlantic margin, *Nat. Geosci.*, *7*, 657–661, doi:10.1038/ngeo2232.
Sloan, E. D., and C. A. Koh (2008), *Clathrate Hydrates of Natural Gases*, 3rd ed., CRC Press, Boca Raton, Fla.
Solomon, E. A., M. Kastner, I. R. MacDonald, and I. Leifer (2009), Considerable methane fluxes to the atmosphere from hydrocarbon seeps in the Gulf of Mexico, *Nat. Geosci.*, *2*(8), 561–565, doi:10.1038/ngeo574.
Sriskantharajah, S., R. E. Fisher, D. Lowry, T. Aalto, J. Hatakka, M. Aurela, T. Laurila, A. Lohila, E. Kuitunen, and E. G. Nisbet (2012), Stable carbon isotope signatures of methane from a Finnish subarctic wetland, *Tellus, Ser. B*, *64*, 18818, doi:10.3402/tellusb.v64i0.18818.
Steinle, L., et al. (2015), Water column methanotrophy controlled by a rapid oceanographic switch, *Nat. Geosci.*, *8*(5), 378–382, doi:10.1038/ngeo2420.
Sundermeyer, M. A., and J. F. Price (1998), Lateral mixing and the North Atlantic Tracer Release Experiment: Observations and numerical simulations of Lagrangian particles and a passive tracer, *J. Geophys. Res.*, *103*(C10), 21,481–21,497, doi:10.1029/98JC01999.
Teigen, S. H., F. Nilsen, and B. Gjevik (2010), Barotropic instability in the West Spitsbergen Current, *J. Geophys. Res.*, *115*, C07016, doi:10.1029/2009JC005996.
Thatcher, K. E., G. K. Westbrook, S. Sarkar, and T. A. Minshull (2013), Methane release from warming-induced hydrate dissociation in the West Svalbard continental margin: Timing, rates, and geological controls, *J. Geophys. Res. Solid Earth*, *118*, 22–38, doi:10.1029/2012JB009605.
Wanninkhof, R. (1992), Relationship between wind speed and gas exchange over the ocean, *J. Geophys. Res.*, *97*(C5), 7373–7382, doi:10.1029/92JC00188.
Wanninkhof, R., W. E. Asher, D. T. Ho, C. Sweeney, and W. R. McGillis (2009), Advances in quantifying air-sea gas exchange and environmental forcing, *Annu. Rev. Mar. Sci.*, *1*, 213–244, doi:10.1146/annurev.marine.010908.163742.
Westbrook, G. K., et al. (2009), Escape of methane gas from the seabed along the West Spitsbergen continental margin, *Geophys. Res. Lett.*, *36*, L15608, doi:10.1029/2009GL039191.
Wiesenburg, D. A., and N. L. J. Guinasso (1979), Equilibrium solubilities of methane, carbon monoxide, and hydrogen in water and sea water, *J. Chem. Eng. Data*, *24*(4), 356–360, doi:10.1021/je60083a006.